Scaling of strength and lifetime probability distributions of quasibrittle structures based on atomistic fracture mechanics

Zdeněk P. Bažant[a,1], Jia-Liang Le[a], and Martin Z. Bazant[b]

[a]Department of Civil Engineering and Materials Science, Robert R. McCormick School of Engineering and Applied Science, Northwestern University, Evanston, IL 60208-3109; and [b]Department of Chemical Engineering, Massachusetts Institute of Technology, Cambridge, MA 02139-4307

Contributed by Zdeněk P. Bažant, April 30, 2009 (sent for review January 27, 2009)

The failure probability of engineering structures such as aircraft, bridges, dams, nuclear structures, and ships, as well as microelectronic components and medical implants, must be kept extremely low, typically $<10^{-6}$. The safety factors needed to ensure it have so far been assessed empirically. For perfectly ductile and perfectly brittle structures, the empirical approach is sufficient because the cumulative distribution function (cdf) of random material strength is known and fixed. However, such an approach is insufficient for structures consisting of quasibrittle materials, which are brittle materials with inhomogeneities that are not negligible compared with the structure size. The reason is that the strength cdf of quasibrittle structure varies from Gaussian to Weibullian as the structure size increases. In this article, a recently proposed theory for the strength cdf of quasibrittle structure is refined by deriving it from fracture mechanics of nanocracks propagating by small, activation-energy-controlled, random jumps through the atomic lattice. This refinement also provides a plausible physical justification of the power law for subcritical creep crack growth, hitherto considered empirical. The theory is further extended to predict the cdf of structural lifetime at constant load, which is shown to be size- and geometry-dependent. The size effects on structure strength and lifetime are shown to be related and the latter to be much stronger. The theory fits previously unexplained deviations of experimental strength and lifetime histograms from the Weibull distribution. Finally, a boundary layer method for numerical calculation of the cdf of structural strength and lifetime is outlined.

cohesive fracture | crack growth rate | extreme value statistics | size effect | multiscale transition

A comprehensive theory of the statistical strength distribution exists only for perfectly brittle structures failing at macrocrack initiation from a negligibly small representative volume element (RVE) of material. The objective of the present article is to extend recent studies (1–3) by developing a comprehensive and atomistically based theory for strength and lifetime distributions of structures consisting of quasibrittle materials. These materials, which include fiber composites, concretes, rocks, stiff soils, foams, sea ice, consolidated snow, bone, tough industrial and dental ceramics, and many other materials on approach to nanoscale, are characterized by a RVE that is not negligible compared with structure size D. The space does not allow commenting on previous valuable contributions made by Coleman (4), Zhurkov (5, 6), Freudenthal (7), Phoenix (8, 9) and others (10, 11) (for such comments, see, e.g., refs. 2, 3, 12, and 13).

Fracture Kinetics on Atomic Scale. Consider a nano-scale size atomic lattice block undergoing fracture (Fig. 1*A*). The separation δ between the opposite atoms across the crack gradually increases by smallincrements as the distance from the crack front grows. The work of the force F_b transmitted across each pair of opposite atoms on their relative displacement δ defines a certain local potential $\Pi_1(\delta)$, which is a part of the overall potential function Π (or free energy) of the atomic lattice block. The equilibrium states of these atomic pairs (bonds) are marked on the local potential curves $\Pi_1(\delta)$ by circles. As the fracture separation grows from one atomic pair to the next, the state marked by the circle moves on the curve $\Pi_1(\delta)$ up and right (Fig. 1*B*). These states are also shown on the corresponding curves of bond force $F_b(\delta) = \partial\Pi_1/\partial\delta$ between the opposite atoms in each pair (Fig. 1*C*). The local bond failure begins when the peak point of the curve $F_b(\delta)$ is reached. This point corresponds to the point of maximum slope of the curve $\Pi_1(\delta)$ (state 3), and represents the end of the cohesive crack [an old idea attributed to Barenblatt (14)]. The true crack ends at the pair where the bond force is reduced to 0 (state 1).

The fracture process zone (FPZ) in the lattice spans approximately from state 1 to state 3, which lies many atoms apart. As the fracture propagates, the diagram $P(u)$ of load $P = \partial\Pi/\partial u$ applied on the atomic lattice block versus the associated displacement u caused by elasticity of lattice and by fracture growth would have the usual shape shown in Fig. 1*D* if the lattice were treated as a continuum (the curvature of the rising portion is caused by finiteness of the length of growing FPZ). On the nanoscale, however, the lattice is not a continuum. The fracture advances by random jumps over the activation energy barriers Q on the surface of the state potential Π (free energy) of the atomic lattice block. These barriers cause the diagram $P(u)$ to be wavy; see Fig. 1*E*, where the radial lines marked as $a_1, a_2, \ldots$ correspond to the unloading lines for subsequent crack lengths ending at different atomic pairs marked in Fig. 1*A*.

The interatomic crack propagates by jumps equal to the atomic spacing δ_a. During each jump, one barrier on the potential Π as a function of u must be overcome (see the wavy potential profile in Fig. 1*G*). After each jump, at each new crack length, there is a small decrease (Fig. 1 *F* and *G*) of the overall potential Π of the atomic lattice block, corresponding to a small advance along the load-deflection curve $P(u)$ (Fig. 1*E*). An important point is that the separation of opposite atoms (in their equilibrium positions) increases during each jump by only a small fraction of their initial distance δ_a.

Because of thermal activation, the states of the atomic lattice block fluctuate and can jump over the activation energy barrier in either direction (forward of backward, Fig. 1*F*), although not with the same frequency. When crack length a (defined by the location of state 3 in Fig. 1 *A–C*) jumps by one atomic spacing, i.e, from a_i to $a_i + \delta_a$, $i = 1, 2, 3, \ldots$), the activation energy barrier Q changes by a small amount, ΔQ, corresponding to the energy release by fracture (Fig. 1 *F* and *G*) that is associated with the equilibrium load drop P caused by fracture (Fig. 1 *E*).

To calculate ΔQ, consider planar 3-dimensional cracks that grow in an affine, or self-similar, manner (e.g., expanding concentric circles or squares). The FPZ of the lattice crack cannot be expected to be negligible compared with the size l_a of the atomic

Author contributions: Z.P.B. designed research; Z.P.B., J.-L.L., and M.Z.B. performed research; J.-L.L. analyzed data; and Z.P.B. and J.-L.L. wrote the paper.

The authors declare no conflict of interest.

[1]To whom correspondence should be addressed. E-mail: z-bazant@northwestern.edu.

www.pnas.org/cgi/doi/10.1073/pnas.0904797106

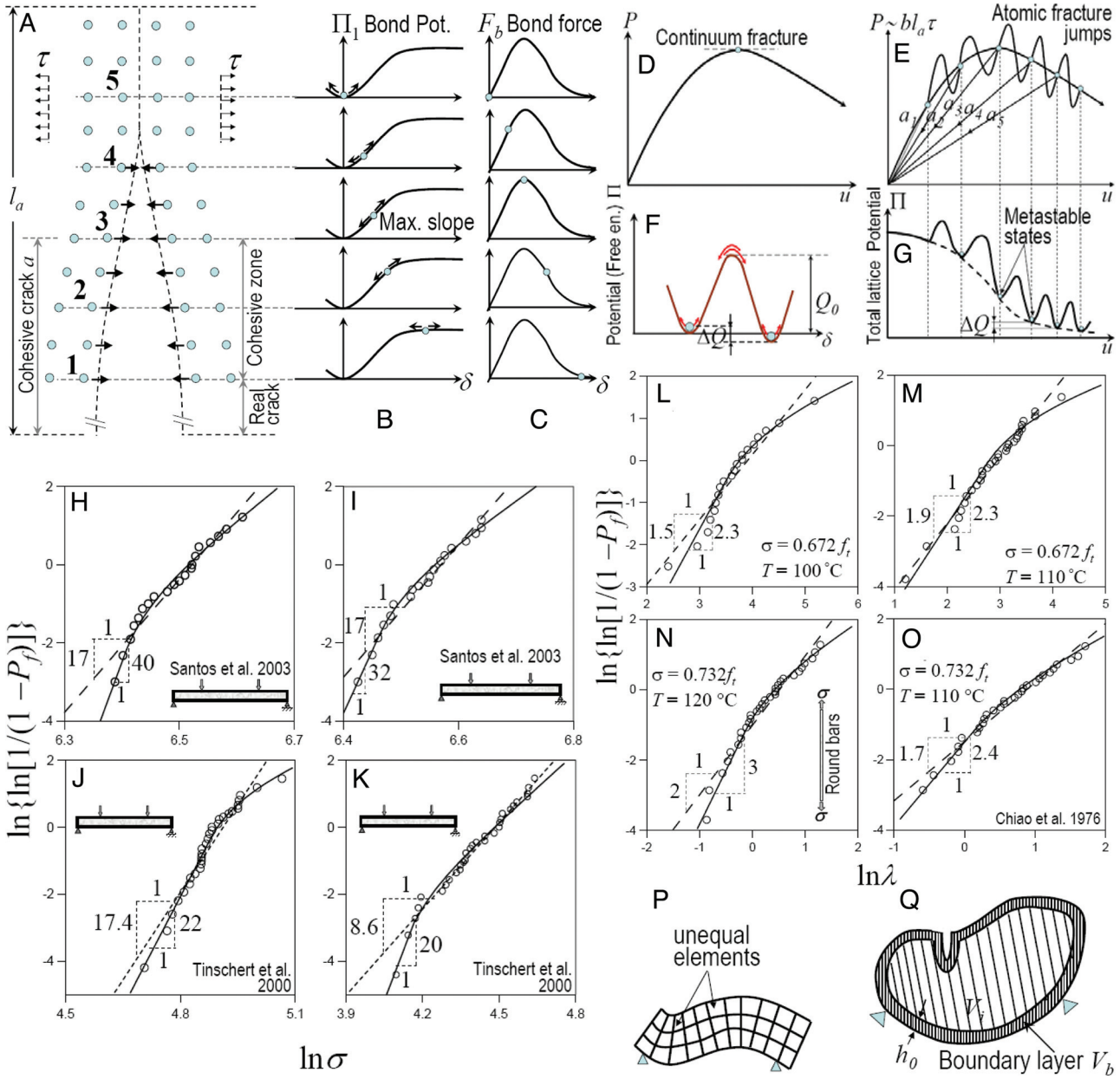

Fig. 1. Nanoscale fracture and fits of histograms. (*A–C*) Fracture of atomic lattice. (*D–G*) Load-displacement curve of atomic lattice block. (*H–K*) Optimum least-squares fits of experimental strength histograms by the present theory and the 2-parameter Weibull distribution: (*H*) Sintered Si_3N_4 with CTR_2O_3/Al_2O_3 additives, (*I*) sintered Si_3N_4-Al_2O_3-Y_2O_3, (*J*) Vitadur Alpha Core, (*K*) Leucite-reinforced porcelain. (*L–O*) Optimum least-squares fits of experimental lifetime histograms of Kevlar 49 fiber composites by the present theory and the 2-parameter Weibull distribution. (*P*) Problematic subdivision for curved boundary. (*Q*) Nonlocal boundary layer model.

lattice block, and so we will use the approximation of equivalent linear elastic fracture mechanics (LEFM) in which the tip of an equivalent sharp LEFM crack is considered to lie approximately in the middle of the FPZ. The LEFM stress intensity factor (of mode I, II, or III) is in general expressed as $K_a = \tau\sqrt{l_a}k_a(\alpha)$, where $\alpha = a/l_a$ = relative crack length, $k_a(\alpha)$ = dimensionless stress intensity factor, $\tau = c\sigma$ = remote stress applied on the nanoscale on the atomic lattice block of size l_a (Fig. 1*A*); c is a nano-macro stress concentration factor; and σ = macroscale stress in the RVE. For a circular (or penny-shaped) crack of radius a loaded in mode I by a remote stress, $k_a(\alpha) = \sqrt{4\alpha/\pi}$.

The energy release rate of the crack (with respect to crack length rather than time), per unit length of crack perimeter, is $\mathcal{G}_a(\alpha) = K_a^2/E_1 = k_a^2(\alpha)l_a\tau^2/E_1$. Here E_1 = Young's (elastic) modulus for a continuum approximation of the lattice (which is larger than the macroscopic Young's modulus E); $k_a^2(\alpha)$ represents the dimensionless energy release rate function of LEFM for continuous bodies, characterizing the geometry of fracture and of the atomic lattice block (15) (if the block boundaries are distant, $k_a^2(\alpha) \propto \gamma\alpha$). Let γ_1 = geometry constant such that $\gamma_1 a = \gamma_1\alpha l_a$ = crack perimeter, the crackbeing assumed to grow radially in an affine manner ($\gamma_1 = 2\pi$ for a circular crack of radius $a = \alpha l_a$, and $\gamma_1 = 8$ for a square perimeter crack). Similar to the expression in ref. 3 (derived by assuming 2- rather than 3-dimensional cracks), the increment of energy that is released when the crack advances by δ_a along its entire perimeter of length $\gamma_1\alpha l_a$ is:

$$\Delta Q = \delta_a\left[\frac{\partial\Pi^*(P,a)}{\partial a}\right]_P = \delta_a(\gamma_1\alpha l_a)\mathcal{G}_a = V_a(\alpha)\frac{\tau^2}{E_1} \qquad [1]$$

Here, Π^* = complementary energy potential (Gibbs' free energy) of the atomic lattice block, and $V_a(\alpha) = \delta_a(\gamma_1\alpha l_a^2)k_a^2(\alpha)$ = activation volume. [Note that if the stress tensor is written as $\tau\, \boldsymbol{s}$, where τ = stress parameter, one may write $\mathbf{V}_a = \boldsymbol{s} : \boldsymbol{v}_a$, where $\boldsymbol{v}_a$ = activation volume tensor, as in the atomistic theories of phase transformations in crystals (16).]

Because the cohesive crack is much longer than δ_a, the separation δ changes very little during each crack jump by one atomic spacing δ_a, and so the activation energy barrier for a forward jump, $Q_0 - \Delta Q/2$, differs very little from the activation energy barrier for a backward jump, $Q_0 + \Delta Q/2$ (Q_0 = activation energy at no stress) (Fig. 1*F*). Note that multiple activation energy barriers $Q_0 = Q_1, Q_2, \ldots$ are always present; however, the lowest one always dominates. The reason is that the factor $e^{-Q_1/kT}$ is very small, typically 10^{-12} (e.g., if $Q_2/Q_1 = 1.2$ or 2, then $e^{-Q_2/kT} = 0.0043e^{-Q_1/kT}$ or $10^{-23}e^{-Q_1/kT}$ and thus makes a negligible contribution; and if $Q_2/Q_1 = 1.02$, then Q_1 and Q_2 can be replaced by a single activation energy $Q_0 = 1.01Q_1$). Consequently, the jumps from one metastable state to the next on the surface of the atomic lattice block potential Π^* must be happening in both forward and backward directions, although at slightly different frequencies. According to the transition rate theory (17, 18), the first-passage time for each transition (in the limit of a large free-energy barrier, $Q_0 \gg kT$) is given by Kramer's formula (19). Thus, the net frequency of crack length jumps is (3):

$$f_1 = \nu_T(e^{(-Q_0+\Delta Q/2)/kT} - e^{(-Q_0-\Delta Q/2)/kT}) \quad [2]$$

$$= 2\nu_T e^{-Q_0/kT}\sinh[V_a(\alpha)/V_T] \quad [3]$$

where $V_T = 2E_1kT/\tau^2$; ν_T is the characteristic attempt frequency for the reversible transition, $\nu_T = kT/h$, where $h = 6.626 \cdot 10^{-34}$ Js = Planck constant = (energy of a photon)/(frequency of its electromagnetic wave); T = absolute temperature; and $k = 1.381 \cdot 10^{-23}$ J/K = Boltzmann constant. Since δ_a is of the order of 0.1 nm, $V_a \sim 10^{-26}$ m^3. Volume V_T depends on $\tau = c\sigma$ where c is expected to be >10. For example, in the nanostructure of hardened Portland cement gel, the nanoscale remote stress may perhaps be $\tau \approx 20$ MPa, which gives $V_T \sim 10^{-25}$ m^3, and so $V_a/V_T \ll 1$. Therefore, Eq. **3** becomes $f_1 \approx e^{-Q_0/kT}[\nu_T V_a(\alpha)/kT]\tau^2/E_1$. Denoting $H_T = e^{-Q_0/kT}(\delta_a l_a^2/E_1 h)$ and $F_T = \gamma_1\alpha k_a^2(\alpha)H_T$, we thus have:

$$f_1 = F_T\tau^2 \quad [4]$$

The fact that frequency f_1 is a power law of stress τ with a zero threshold is essential for the forthcoming arguments. Important for the foregoing derivation is that $\Delta Q \ll kT \ll Q_0$ or $\tau \ll (E_1kT/V_a)^{1/2}$. Another noteworthy point is that stress-independent crack front diffusion (as a random walk) should be negligible because the Péclet number $\mathrm{Pe} \gg 1$ [$\mathrm{Pe} = 2f_1 l_a/\delta_a f = 4(l_a/\delta_a)(V_a/V_T)$, where $f = \nu_T e^{-Q_0/kT}$].

In classical macroscale continuum fracture, by contrast, the jumps representing fracture reversal play no role because the crack face separations of interest equal many atomic spacings, rather than a small fraction of one atomic spacing; ΔQ is thus entirely negligible and the free-energy change is smooth (as shown in Fig. 1*G*) (this point was made in ref. 20, figure 1.18).

Failure Frequency and Probability at Nanoscale. The atomic lattice fails when the nanocrack propagates from its original length a_0 to a certain critical length a_c at which the crack looses stability and propagates dynamically [this occurs at the point of the $P(u)$ curve in Fig. 1*E* where the downward tangent slope becomes equal in magnitude to the stiffness of embedment of the lattice block in the surrounding microstructure (21)]. To get to a_c, the crack experiences many length jumps, say n jumps, where the frequency of each jump is given by Eq. **4**. At the atomic lattice scale, it may be assumed, in general, that each jump is independent (i.e., the frequency of the jump is independent of the particular history of breaking and restoration sequences that brought the nanocrack to the current length) (20). The failure probability of the atomic lattice on sudden application of stress can thus be written as $P_f(\tau) \propto \lim_{n\to\infty}\sum_{i=1}^{n} f_{1(i)} = \int_{\alpha_0}^{\alpha_c} f_1 \mathrm{d}\alpha$, where $f_{1(i)}$ = value of f_1 for crack length $a_{(i)}$ ending at interatomic bond number i. Denoting $C_T = H_T\gamma_1\int_{\alpha_0}^{\alpha_c}\alpha k_a^2(\alpha)\mathrm{d}\alpha$, we thus get

$$P_f(\tau) \propto C_T\tau^2 \quad [5]$$

Nano-Macro Transition of Failure Probability. We consider the broad class structures that fail as soon as a macrocrack initiates from one RVE (15, 22, 23) (they are called the positive geometry structures, characterized by $\partial K/\partial a > 0$; K = stress intensity factor). Their strength is statistically modeled by a chain of RVEs, i.e., by the weakest-link model. However, in contrast to Weibull theory, the number of RVEs (or links in the chain) is not infinite because the RVE size is not negligible. For softening damage and failure, and in contrast to the homogenization theory, the RVE must be defined as the smallest material volume whose failure triggers the failure of the whole structure (1). Typically, the RVE size l_0 is ≈2 to 3 inhomogeneity sizes (2, 25).

The transition from the nanoscale of atomic lattice crack to the macroscale of RVE can be represented, for statistical purposes, by a hierarchy of series and parallel couplings (i.e., chains of links and bundles of fibers) (see ref. 1, figure 1*E*). In such couplings, a power law tail of strength cumulative distribution function (cdf) is indestructible (2). The series couplings preserve the tail exponent and extend the reach of the power-law tail. In parallel couplings, the tail exponents of the elements are additive [as proven for both brittle (2, 24) and plastic or softening elements (2)], and the reach of the power-law tail shortens drastically. The cdf of strength of one RVE can be approximated by a Gaussian core onto which a far-left Weibull tail is grafted at failure probability $P_{gr} \approx 10^{-4} - 10^{-3}$ (ref. 1, equations 6 and 7) [in more detail (2)]. The meaning of Weibull modulus m, which is typically 10 to 50, is the minimum of the sum of the Weibull tail powers among all possible cuts separating the hierarchical model into two halves.

The elements of the hierarchical model may be imagined to represent atomic lattice cracks, for which the tail exponent of strength cdf is 2 (Eq. **5**). Isn't that in conflict with the preceding simpler model (1), in which the elements of the hierarchical model had the tail exponent of 1? No, because the elements in ref. 1 represented the break of a bond between a pair of atoms, which occurs one scale lower than the break of atomic lattice block. According to the hierarchical model, the passage from that scale to the scale of atomic lattice should raise the exponent, and the present analysis shows it should raise it to 2. Although refs. 1 and 2 led to equivalent results on the RVE level, the treatment of interatomic pair breaks in refs. 1 and 2 was oversimplified because the present near-symmetry of forward and backward activation energy barriers $Q_0 \pm \Delta Q$ does not exist for isolated atomic pairs. Fracture mechanics of the atomic lattice (Eq. **4**), as introduced here and in ref. 3, is essential.

Size Effect on Strength Distribution. The chain of N RVEs survives if all its elements survive. So, according to the joint probability theorem, and under the hypothesis of independent random variables the failure probability of the structure, P_f, follows the equation:

$$1 - P_f(\sigma_N) = \prod_{i=1}^{N}\{1 - P_1[\sigma_i(\boldsymbol{x}_i)]\} \quad [6]$$

Here, $\sigma_N = c_g P_{\max}/bD$ = nominal strength of structure (22, 23, 25), b = structure width, and c_g = arbitrarily chosen dimensionless geometry parameter (for a suitable choice of c_g, σ_N = maximum

normal stress in the structure); $\sigma_i(\boldsymbol{x}_i) = \sigma_N s(\boldsymbol{x}_i)$ = maximum principal macroscale stress at the center $\boldsymbol{x}_i$ of the ith RVE; $s(\boldsymbol{x})$ = dimensionless stress field; $P_1(\sigma)$ = grafted Gauss–Weibull cdf of the strength of a single RVE (ref. 1, equations 6 and 7).

As N increases, the Weibull tail gradually spreads and the Gaussian portion of cdf shrinks until virtually the entire cdf becomes Weibullian, which means that the structure becomes brittle and occurs when the equivalent number of RVEs $N_{\text{eq}} \geq N_b$, where $N_b = 5/P_{gr}$ (typically 5×10^3). For $N_{\text{eq}} < N_b$, P_f must be computed from Eq. **6** (N_{eq} results by scaling N according to the stress field (1, 2); for a homogeneous stress field, $N_{\text{eq}} = N$).

Macrocrack Growth Law as Consequence of Subcritical Nanocrack Growth Rate. To predict the lifetime of structures, we need to know the frequency of crack jumps that governs the rate of growth, $\dot{a}$, of the atomic crack. According to Eq. **4**, $\dot{a} = \delta_a f_1$ or

$$\dot{a} = \nu_1 e^{-Q_0/kT} K^2 \qquad [7]$$

where $\nu_1 = \delta_a^2(\gamma_1 \alpha l_a)/E_1 h$. On the macroscale, a power law for the crack growth rate has been proposed (10, 15, 26–29). It reads:

$$\dot{a} = A e^{-Q_0/kT} K^n \qquad [8]$$

where A, n = positive empirical constants, K = stress intensity factor at macroscale, and a = length of macrocrack. Experiments show n to range from 10 to 30 (10, 26). Eq. **8** implies environmental and thermal effects on creep crack growth, entering through the Arrhenius factor $e^{-Q_0/kT}$.

Eqs. **7** and **8** have different exponents but the same form, except that, unlike A, factor ν_1 depends on the length of nano-crack. However, the FPZ does not change significantly as it travels through the structure (which is a central tenet behind the constancy of G_f). Therefore, all the different relative crack lengths α in the nanostructure of a FPZ must average out to give a constant A, which is independent of the length of macrocrack. Note that parameter A depends on structure size [just like the size effect on Paris' law (15)].

To explain the difference in exponents, we may use the condition that the energy dissipation power of the macroscale crack a must be equal to the combined energy dissipation power of all the active nanocracks a_i ($i = 1, \ldots N$) in the FPZ of the macroscale crack. So, $(\partial \Pi^*/\partial a)\dot{a} = \sum_i (\partial \Pi^*/\partial a_i)\dot{a}_i$, or

$$\mathcal{G}\dot{a} = \sum_{i=1}^{N} \mathcal{G}_i \dot{a}_i \qquad [9]$$

where $\mathcal{G}$ and $\mathcal{G}_i$ denote the energy release rates with respect a and a_i. By expressing the energy release rate in terms of the stress intensity factor and substituting Eq. **7** for $\dot{a}_i$, we get

$$\dot{a} = e^{-Q_0/kT}\phi(K) \quad \text{where:} \quad \phi(K) = \sum_{i=1}^{N} \frac{\nu_i K_i^4 E}{K^2 E_i} \qquad [10]$$

where K_i = stress intensity factor of nanocrack a_i, E_i = elastic modulus of atomic lattice containing nanocrack a_i, and $\nu_i = \delta_a^2(\gamma_1 \alpha_i l_i)/E_i h$. In the context of linear elasticity, one may assume: $K_i = \omega_i K$ where ω_i are some constants. Hence, one may rewrite $\phi(K)$ as:

$$\phi(K) = K^2 \sum_{i=1}^{N} \frac{\nu_i \omega_i^4 E}{E_i} \qquad [11]$$

This equation is the key to the multiscale transition of fracture kinetics. The number of active nanocracks N in the FPZ of the macrocrack can be calculated in a multiscale manner: The FPZ of a macrocrack contains q_1 mesocracks, each of which contains a meso-FPZ with q_2 microcracks, each of which again contains a micro-FPZ with q_3 submicrocracks, ... and so forth, all the way down to the atomic lattice scale. So, if the multiscaling from macro to nano bridges s scales, the number of nanocracks contained in the macro-FPZ is: $N = q_1 q_2 \cdots q_s$.

On each material scale, the number of activated cracks q within the FPZ of the next higher scale μ must be a function of the relative stress intensity factor K/K_μ, i.e., $q = q(K/K_\mu)$, where K_μ = critical value of K for cracks of scale μ. It may be expected that the function $q(K/K_\mu)$ increases rapidly with increasing K, whereas the ratio $\nu_i \omega_i^4 E/E_i$ varies far less. Therefore, one may replace E_i, ω_i, and ν_i by some effective mean values E_a, ω_a, and ν_a : $\phi(K) = \nu_a \omega_a^4 (E/E_a) K^2 \prod_{\mu=1}^{s} q(K/K_\mu)$.

Since there appears to be no characteristic value of K at which the behavior of $q(K/K_\mu)$ would qualitatively change, function $q(K/K_\mu)$ should be self-similar, i.e., a power law, $q(K/K_\mu) = (K/K_\mu)^r$. Consequently, function $\phi(K)$ should be a power law as well:

$$\phi(K) = \frac{\nu_a \omega_a^4 E}{E_a \left(\prod_\mu K_\mu^r\right)} K^{rs+2} \qquad [12]$$

Setting $rs + 2 = n$ and substituting $\phi(K)$ back to Eq. **10**, one thus finally obtains the power law for macrocrack growth.

According to the foregoing arguments, the main reason why the power-law exponent of crack growth rate increases from 2 at the atomic scale to $n \approx 10$ to 30 at the macro-scale is that the number N of energy dissipating nanocracks steeply increases with the applied macrostress. Nevertheless, these arguments merely constitute a plausible explanation but not proof. The fact that they deliver agreement with experiments is essential.

Distribution of Structural Lifetime. Consider load histories in which applied stress σ is first raised rapidly to a value σ_0 less than the short-time strength, then is held constant for a certain time period Δt, and after that is raised rapidly up to failure, occurring at stress σ^*. When Δt is increased from 0 to arbitrarily large periods of time, there is a continuous transition of failure stress σ^* from the short-time failure stress σ_N, obtained in a typical laboratory strength test, to failure stress $\sigma^* = \sigma_0$ obtained in a test of lifetime λ at constant stress σ_0. Therefore, the same failure criterion, based on the same theory, must apply to the short-time strength and to the lifetime.

Now consider a dominant subcritical macrocrack of length a_R growing within the RVE. Its stress intensity factor may be expressed as $K = \sigma\sqrt{l_0}k(\alpha_R)$, where $\alpha_R = a_R/l_0$, and l_0 = RVE size. To relate the statistics for long-time loading and rapid loading, the use of crack growth law (Eq. **8**) is crucial. For the case of rapid loading (strength test), one has $\sigma = rt$ (r = loading rate). By integrating Eq. **8**, one obtains:

$$\sigma_N^{n+1} = r(n+1)e^{Q_0/kT} I \qquad [13]$$

where $I = A^{-1} l_0^{1-n/2} \int_{\alpha_0}^{\alpha_c} k^{-n}(\alpha) \mathrm{d}\alpha$. Because the lifetimes of interest are normally much longer than the duration of laboratory strength tests, the sustained stress σ_0 is generally very low compared with the mean strength of the RVE. Therefore, the initial rapidly increasing portion of the load history makes a negligible contribution to the structural lifetime, λ. By integrating Eq. **8** at constant σ_0, one obtains:

$$\sigma_0^n \lambda = e^{Q_0/kT} I, \qquad [14]$$

Eliminating I from Eqs. **13** and **14**, one gets the following simple relationship between σ_N and λ:

$$\sigma_N = \beta \sigma_0^{n/(n+1)} \lambda^{1/(n+1)} \qquad [15]$$

where $\beta = [r(n+1)]^{1/(n+1)}$ = constant.

Eq. **15** makes it possible to calculate the cdf of lifetime of one RVE from the cdf of strength of the RVE, defined as Gauss–Weibull grafted distribution in equations 6 and 7 of ref. 1. The result is

$$\text{for } \lambda < \lambda_{gr} : P_1(\lambda) = 1 - \exp[-(\lambda/s_\lambda)^{m/(n+1)}]; \quad \textbf{[16]}$$

$$\text{for } \lambda \geq \lambda_{gr} : P_1(\lambda) = P_{gr} + \frac{r_f}{\delta_G\sqrt{2\pi}} \int_{\lambda_1}^{\lambda_2} e^{-(\lambda'-\mu_G)^2/2\delta_G^2} d\lambda' \quad \textbf{[17]}$$

where $\lambda_{gr} = \beta^{-(n+1)}\sigma_0^{-n}\sigma_{N,gr}^{n+1}$, $\lambda_1 = \gamma\lambda_{gr}^{1/(n+1)}$, $\lambda_2 = \gamma\lambda^{1/(n+1)}$, $\gamma = \beta\sigma_0^{n/(n+1)}$, $s_\lambda = s_0^{n+1}\beta^{-(n+1)}\sigma_0^{-n}$, and μ_G, δ_G, s_0 are statistical parameters for the strength cdf as defined in equations 6 and 7 of ref. 1. For one RVE, the cdfs of both strength and lifetime have Weibullian tails, but with very different exponents. The Weibull modulus for the lifetime cdf is

$$m_\lambda = \frac{m}{n+1} \quad \textbf{[18]}$$

which is significantly lower than the Weibull modulus m for the strength cdf. However, the grafting probability P_{gr} is the same for both. In contrast to the core of strength cdf, the core of lifetime cdf is not even approximately Gaussian.

Based on the finite chain model, the lifetime distribution of a structure can be calculated from the joint probability theorem:

$$P_f(\lambda, \sigma_0) = 1 - \prod_{i=1}^{n}[1 - P_1(\lambda, \sigma_0 s(\boldsymbol{x}_i))] \quad \textbf{[19]}$$

Similar to the size effect on the cdf of strength, the lifetime distribution of large structures depends only on the tail of the lifetime cdf of one RVE. As the structure size is increased, the cdf of lifetime of the whole structure will eventually converge to the Weibull cdf, i.e., $P_f(\lambda) = 1 - \exp[-(\lambda/S)^{m/(n+1)}]$.

Optimum Fitting of Strength and Lifetime Histograms. The observed strength histograms for ceramics, concrete, and fiber composites (10, 30, 31) typically exhibit in Weibull scale a kink that separates two segments. The lower segment is a Weibull straight line and the upper one deviates from this line to the right. These histograms have often been fitted by the 2-parameter Weibull distribution, which has a zero threshold. However, systematic deviations always occurred unless the data were too few and the structure size $\gg$ RVE.

Fig. 1 *H–K* documents further close fits of histograms of flexural strength of various industrial and dental ceramics (32–34). Previous investigators fitted them closely by the 3-parameter Weibull distribution with a nonzero threshold, though with unreasonably small Weibull moduli m. It is now clear that close fits were possible because only a few hundred tests were made. Weibull' s data for concrete (30) (with about 5,000 tests still being the most extensive to date) cannot be fitted closely by the 3-parameter Weibull distribution (ref. 2, figure 3d). Further similar histograms of ceramics have also been fitted closely by the present theory (12, 13).

In logarithmic plots of size effect on the mean structural strength, the Weibull theory gives a straight line, whereas tests show a large upward deviation for smaller sizes; see figure 1q in ref. 23 for concrete and figure 2b in ref. 35 for laminates. As for ceramics, unfortunately, no size effect tests accompanied the histogram testing, although it would have been the easiest way to detect the inadequacy of Weibull distribution.

Fig. 1 *L–O* documents that the present theory fits closely the lifetime histograms of organic fiber (Kevlar 49) composites (36), whereas the 2-parameter Weibull cdf does not. The test temperatures were 100–110°C. The specimens were bars under uniform uniaxial tensile stress equal to ≈70% of the mean strength of the specimen.

Similar to the strength histograms, the lifetime histograms in Weibull plots are again found to have two segments separated by a kink, which cannot be fitted by the 2-parameter Weibull distribution. The present theory fits the entire histograms well. The lower segment is a straight line, whose slope represents the Weibull modulus m_λ. The fits show that $m_\lambda \approx 2.3$–3, which is significantly lower than Weibull modulus m of the strength distribution [for Kevlar 49 fiber composites, typically m = 40–50 (8)]. From Eq. **18**, the crack growth rate exponent $n \approx 16$.

Effective Experimental Determination of Weibull Modulus of Lifetime Distribution. Determining the Weibull modulus of lifetime distribution by histogram testing is time consuming and costly and is rendered unnecessary by Eq. **18**. One merely needs the Weibull modulus m of the strength distribution, which is best determined from mean size effect tests (13). The crack growth rate exponent n can then be obtained by standard tests that measure the subcritical crack growth velocity.

Size Effect on Mean Structural Strength and Lifetime. The mean of strength as well as lifetime for a structure with any number of RVEs may be calculated as $\bar{x} = \int_0^\infty [1 - P_f(x)]dx$, where $x = \sigma_N$ for strength distribution, $x = \lambda$ for lifetime distribution, and $P_f(x)$ = strength or lifetime cdf of a structure. It is impossible to express $\bar{\sigma}_N$ and $\bar{\lambda}$ analytically, but the asymptotes can be determined. For small sizes, the curves of size effect on the mean strength and lifetime deviate from the power-law size effect of the Weibull theory. The deviation is caused by the fact that the fracture process zone size is not negligible compared with the structure size. The predicted curve of size effect on the mean specimen strength is found to agree well with the mean size effect tests (22, 37) and with the predictions by other established mechanical models such as the cohesive crack model (15, 22, 38), crack band model (15), and nonlocal damage model (39). The mean size effect on strength [Type 1 size effect (23)] can be well approximated by the formula (25, 40):

$$\bar{\sigma}_N = [(N_a/D) + (N_b/D)^{r/m}]^{1/r} \quad \textbf{[20]}$$

where m, r, N_a, N_b = constants. The m-value is best identified by tests of size effect on strength, and it must match the slope of the left tail of strength histograms. To identify r, N_a and N_b, one needs to solve three simultaneous equations expressing three asymptotic matching conditions for $[\bar{\sigma}_N]_{D\to l_0}$, $[d\bar{\sigma}_N/dD]_{D\to l_0}$, and $[\bar{\sigma}_N D^{1/m}]_{D\to\infty}$.

The mean strength and lifetime must be related by Eq. **15**. Therefore, the mean size effect on lifetime may be written as:

$$\bar{\lambda} = [(C_a/D) + (C_b/D)^{r/m}]^{(n+1)/r} \quad \textbf{[21]}$$

where m = Weibull modulus of strength cdf, and n = crack growth rate exponent. Parameters C_a, C_b, and r can again be determined by three asymptotic matching conditions. Clearly, the size effect on the mean structural lifetime is far stronger than the size effect on the mean structural strength. This phenomenon is intuitively plausible.

Generalization for Boundary Layer and Nonlocal Interior. Direct use of Eq. **6** to compute P_f is possible if the structure can be subdivided into elements of equal size. Such a subdivision is impossible for general bodies (Fig. 1*P*). One might think of replacing the finite sum corresponding to the weakest-link model with a nonlocal integral over the structure volume V, similar to the nonlocal models for structures with softening distributed damage (39). However, these models lead to troublesome, still unresolved, problems with the treatment of boundaries when the nonlocal integration domain protrudes beyond the body surface.

Therefore, we need a different idea. We separate from the interior volume V_I a boundary layer of thickness $h_0 \approx l_0$ = size of

the RVE. In V_I, a nonlocal continuum treatment is free of trouble since, for the points in V_I, the nonlocal integral domain cannot protrude outside the body surface if it chosen to extend no further than distance h_0 from the center point (Fig. 1*Q*). In the boundary layer, one can introduce nonlocal integration domains for the points of the middle surface, which also cause no trouble with the boundary condition since this surface is closed (i.e., has no boundaries). Eq. **6** thus yields:

$$\ln(1-P_f) = h_0 \int_{\Omega_M} \ln\{1-P_1[\sigma(\boldsymbol{x}_M)]\}\mathrm{d}\Omega(\boldsymbol{x}_M) + \int_{V_I} \ln\{1-P_1[\bar{\sigma}(\boldsymbol{x})]\}\mathrm{d}V(\boldsymbol{x}) \qquad [22]$$

where $P_1(\sigma)$ is the grafted Gauss–Weibull cdf of RVE strength. The first integral runs over all the points $\boldsymbol{x}_M$ of the middle surface Ω_M of the boundary layer, and the second integral runs over all the points $\boldsymbol{x}$ in the interior V_I; and $\bar{\sigma}(\boldsymbol{x})$ is the nonlocal stress at point $\boldsymbol{x}$. When $D/h_0 \to \infty$, the first integral in Eq. **22** becomes negligible, the nonlocal stress $\bar{\sigma}(\boldsymbol{x})$ becomes the local stress $\sigma(\boldsymbol{x})$, and P_f converges to the Weibulldistribution. The same approach, based on Eq. **19**, can be used for the lifetime.

Concluding Remarks. A detailed development of numerical implementation, including the boundary layer theory for quasibrittle failure probability, is beyond the scope of this article and is relegated to a separate article. The present results are bound to impact the safety and lifetime assessments of large load-bearing fiber composite parts for modern fuel-efficient aircraft and ships, and large concrete structures and rock masses. They will also affect the reliability and lifetime assessments of microelectronic devices. If the buildup of residual stresses in the microstructure can be successfully introduced into the formulation, a comprehensive unified theory encompassing also fatigue under cyclic loading is in sight. Finally, note that a mathematically analogous formulation can describe the lifetime statistics of electrical breakdown of gate dielectrics (41).

ACKNOWLEDGMENTS. This work was supported in part by National Science Foundation Grant CMS-0556323 and Boeing, Inc. Grant N007613.

1. Bažant ZP, Pang S-D (2006) Mechanics based statistics of failure risk of quasibrittle structures and size effect on safety factors. *Proc Natl Acad Sci USA* 103:9434–9439.
2. Bažant ZP, Pang S-D (2007) Activation energy based extreme value statistics and size effect in brittle and quasibrittle fracture. *J Mech Phys Solids* 55:91–134.
3. Bažant ZP, Le J-L, Bazant MZ (2008) Size effect on strength and lifetime distributions of quasibrittle structures implied by interatomic bond break activation. *Proceedings 17th European Conference on Fracture (ECF-17), held at Technical University Brno, Brno, Czech Republic*, eds Pokluda J, et al. (European Structural Integrity Society, Brno, Czech Republic), pp 78–92.
4. Coleman BD (1958) Statitics and time dependent of mechanical breakdown in fibers. *J Appl Phys* 29:968–983.
5. Zhurkov SN (1965) Kinetic concept of the strength of solids. *Int J Fract Mech* 1:311–323.
6. Zhurkov SN, Korsukov VE (1974) Atomic mechanism of fracture of solid polymer. *J Polym Sci* 12:385–398.
7. Freudenthal AM (1968) Statstical approach to brittle fracture. *Fracture: An Advanced Treatise*, ed Lievowitz H (Academic, New York), Vol 2, pp 591–619.
8. Phoenix SL (1978) Stochastic strength and fatigue of fiber bundles. *Int J Frac* 14:327–344.
9. Phoenix SL, Tierney L-J (1983) A statistical model for the time dependent failure of unidirectional composite materials under local elastic load-sharing among fibers. *Eng Fract Mech* 18:193–215.
10. Munz D, Fett T (1999) *Ceramics: Mechanical Properties, Failure Behavior, Materials Selection* (Springer, Berlin).
11. Tierney L-J (1983) Asymptotic bounds on the time to fatigue failure of bundles of fibers under local load sharing. *Adv Appl Prob* 14:95–121.
12. Le J-L, Bažant ZP (2009) Finite weakest link model with zero threshold for strength distribution of dental restorative ceramics. *Dent Mater* 25:641–648.
13. Pang S-D, Bažant ZP, Le J-L (2009) Statistics of strength of ceramics: Finite weakest link model and necessity of zero threshold. *Int J Frac*, Special Issue on Physical Aspects of Scaling. 154:131–145.
14. Barenblatt GI (1959) The formation of equilibrium cracks during brittle fracture, general ideas and hypothesis, axially symmetric cracks. *Prikl Mat Mech* 23(3):434–444.
15. Bažant ZP, Planas J (1998) *Fracture and Size Effect in Concrete and Other Quasibrittle Materials* (CRC Press, Boca Raton, FL).
16. Aziz MJ, Sabin PC, Lu GQ (1991) The activation strain tensor: Nonhydrostatic stress effects on crystal growth kinetics. *Phys Rev B* 41:9812–9816.
17. Kaxiras E (2003) *Atomic and Electronic Structure of Solids* (Cambridge Univ Press, New York).
18. Philips, R (2001) *Crystals, Defects and Microstructures: Modeling Across Scales* (Cambridge Univ Press, New York).
19. Risken H (1989) *The Fokker-Plank Equation* (Springer, New York), 2nd Ed.
20. Krausz AS, Krausz K (1988) *Fracture Kinetics of Crack Growth* (Kluwer, Dordrecht, The Netherlands).
21. Bažant ZP, Cedolin L (2003) *Stability of Structures: Elastic, Inelastic, Fracture and Damage Theories* (Dover, New York), Chap 12, 2nd Ed.
22. Bažant ZP (2004) Probability distribution of energetic-statistical size effect in quasibrittle fracture. *Probabil Eng Mech* 19(4):307–319.
23. Bažant ZP (2004) Scaling theory for quasibrittle structural failure. *Proc Natl Acad Sci USA* 101:13400–13407.
24. Phoenix SL, Ibnabdeljalil M, Hui C-Y (1997) Size effects in the distribution for strength of brittle matrix fibrous composites. *Int J Solids Struct* 34:545–568.
25. Bažant ZP (2005) *Scaling of Structural Strength* (Elsevier, London), 2nd Ed.
26. Evans AG (1972) A method for evaluating the time-dependent failure characteristics of brittle materials—and its application to polycrystalline alumina. *J Mater Sci* 7 1137-1146.
27. Thouless MD, Hsueh CH, Evans AG (1983) A damage model of creep crack growth in polycrystals. *Acta Metall* 31:1675–1687.
28. Evans AG, Fu Y (1984) The mechanical behavior of alumina. *Fracture in Ceramic Materials* (Noyes Publications, Park Ridge, NJ), pp 56–88.
29. Bažant ZP, Prat PC (1988) Effect of temperature and humidity on fracture energy of concrete. *ACI Mater J* 85-M32:262–271.
30. Weibull W (1939) The phenomenon of rupture in solids. *Proc R Swedish Inst Eng Res* 153:1–55.
31. Wagner HD (1989) Stochastic concepts in the study of size effects in the mechanical strength of highly oriented polymeric materials. *J Polym Sci* 27:115–149.
32. Santos Cd, et al. (2003) Evaluation of the reliability of Si_3N_4-Al_2O_3-CTR_2O_3 ceramics through Weibull analysis. *Mater Res* 6:463–467.
33. Tinschert J, Zwez D, Marx R, Ausavice KJ (2000) Structural reliability of alumina-, feldspar-, leucite-, mica- and zirconia-based ceramics. *J Dent* 28:529–535.
34. Lohbauer U, Petchelt A, Greil P (2002) Lifetime prediction of CAD/CAM dental ceramics. *J Biomed Mater Res* 63:780–785.
35. Bažant ZP, Zhou Y, Novák D, Daniel IM (2004) Size effect on flexural strength of fiber-composite laminate. *J Eng Mater Technol ASME* 126:29–37.
36. Chiao CC, Sherry RJ, Hetherington NW (1977) Experimental verification of an accelerated test for predicting the lifetime of oragnic fiber composites. *J Comp Mater* 11:79–91.
37. Bažant ZP, Xi Y (1991) Statistical size effect in quasi-brittle structures: II. Nonlocal theory. *J Eng Mech ASCE* 117:2623–2640.
38. Bažant ZP, Vorechovsky M, Novak D (2007) Asymptotic prediction of energetic-statistical size effect from deterministic finite element solutions. *J Eng Mech ASCE* 128:153–162.
39. Bažant ZP, Jirásek M (2002) Nonlocal integral formulations of plasticity and damage: Survey of progress. *J Eng Mech ASCE* 128:1119–1149.
40. Bažant ZP, Novák D (2000) Energetic-statistical size effect in quasibrittle failure at crack initiation. *ACI Mater J* 97:381–392.
41. Le J-L, Bažant ZP, Bazant MZ (2009) Lifetime of high k gate dielectrics under constant voltage and analogy with strength of quasibrittle structures. *T & AM Report 09-06/C6051* (Northwestern Univ, Evanston, IL).